Effects of instrument orientation on small-loop electromagnetic induction surveys of localized 2D conductive targets

2011 J. Geophys. Eng. 8 579

(http://iopscience.iop.org/1742-2140/8/4/010)

IOP Publishing Journal of Geophysics and Engineering
J. Geophys. Eng. **8** (2011) 579–591 doi:10.1088/1742-2132/8/4/010

Effects of instrument orientation on small-loop electromagnetic induction surveys of localized 2D conductive targets

Fabiana Elizabeth Robledo[1,3], **Hilda Patricia Martinelli**[1,2,4] **and Néstor Eduardo Bonomo**[1,2]

[1] Grupo de Geofísica Aplicada y Ambiental, Departamento de Física, Facultad de Ciencias Exactas y Naturales, Universidad de Buenos Aires. Ciudad Universitaria, Pabellón 1, Dto de Física, 1428, Buenos Aires, Argentina
[2] IFIBA (Instituto de Física de Buenos Aires), CONICET (Consejo Nacional de Investigaciones Científicas y Técnicas), Ciudad Universitaria, Pabellón 1 Dto de Fisica, 1428, Buenos Aires, Argentina

E-mail: robledo@df.uba.ar, pmartine@df.uba.ar and bonomo@df.uba.ar

Received 22 February 2011
Accepted for publication 7 October 2011
Published 14 November 2011
Online at stacks.iop.org/JGE/8/579

Abstract
Frequency-domain electromagnetic induction (EMI) systems, composed of two coplanar small coils separated by a fixed distance (EMI or SLEM), enable the rapid detection of a great variety of near-surface structures. One coil generates a controlled, primary magnetic field and the other records the variations of the induced field while the instrument is moved over the studied area. The most usual acquisition configuration corresponds to horizontal coils, with the instrument axis parallel to the prospection lines. Usually, the interpretation is based on the direct visualization of the plan-views of the data measured at each frequency. In addition, to characterize the subsoil structure in-depth, 1D inversion methods are generally applied. The aim of this work is to analyse how the system orientation affects the ability of the method to detect localized, 2D conductive structures, buried at shallow depths, and the possibility of adequately characterizing these targets through 1D inversions. We performed a survey at a test site that contains two known structures of this type, buried in almost perpendicular directions. We performed parallel prospection lines in the direction of each structure, employing, aside from the usual configuration described before, other configurations that included horizontal and vertical coils, with the instrument axis parallel and perpendicular to the lines. For comparison, we also performed a geoelectric dipole–dipole line crossing one of the targets. The features of the anomalies observed in the graphs of the EMI apparent conductivity data strongly depend on the instrument orientation. In the horizontal coil configurations, a decrease of the apparent conductivity is observed just over the targets. Besides, each vertical configuration practically detects only the target aligned with the plane of the coils, as an important positive anomaly. Through numerical simulations, performed using a 2D forward modelling method, we demonstrate that these features are indeed 2D effects associated with the localized character of the studied conductive objects. Then, we applied to the data a 1D inversion method and drawing together the results generated pseudo 3D models of the subsoil. We found that the models obtained for the vertical coil configurations provide better results. They detect the targets as conductive structures and provide a rather good estimation of their depths. Finally, we compare the EMI results with the image obtained from the 2D inversion of the geoelectrical data and analyse the causes of the observed differences.

[3] On a fellowship from Universidad de Buenos Aires.
[4] Author to whom any correspondence should be addressed.

Keywords: electromagnetic induction, small loop, instrument orientation, localized 2D objects, lateral filtering, inversion

(Some figures in this article are in colour only in the electronic version)

1. Introduction

Frequency-domain electromagnetic induction systems composed of two fixed small coils separated by a constant distance, known as EMI (electromagnetic induction) or SLEM (small-loop electromagnetic induction) systems (McNeill 1980, McNeill and Bosnar 1999, Won *et al* 1996, Won 2003) are very sensitive to the presence of structures buried at shallow depths, especially conductive ones. The coils are usually coplanar; one generates a controlled primary magnetic field and the other records the variations of the induced field while the instrument is moved above the studied area at an approximately constant height. These systems are widely used to detect buried metallic bodies, including unexploded ordnance (Miller *et al* 2001, Won *et al* 2001, Butler 2004, Martinelli and Osella 2010), for environmental applications such as contaminant detection and waste site exploration (Sheard *et al* 2005, Auken *et al* 2006, Mitsuhata *et al* 2006, Martinelli and Duplaá 2008, Coria *et al* 2009), and also for archaeological prospecting (Witten *et al* 2003, Osella *et al* 2005, Lascano *et al* 2006, Bongiovanni *et al* 2008) as an alternative method to delimit anomalous zones. A main advantage is that they do not require direct contact with the ground and therefore are much faster than the geoelectric or other electromagnetic methods.

The anomalous zones are determined by direct visualization of data plots. Besides, when the frequency or coil separation can be varied, forward and/or inversion methods can be applied to obtain an approximate quantitative characterization of the anomalies. Even though the usefulness of employing more than one frequency is still under discussion, currently there are many works illustrating how the use of multifrequency responses allows for achieving an improved characterization of the subsoil (Won *et al* 1996, Pellerin and Wannamaker 2005, Bongiovanni *et al* 2008, Martinelli and Duplaá 2008, Martinelli and Osella 2010).

Several methods have been developed to calculate the EMI response of metallic bodies (e.g. Sun *et al* 2004). In these works, the objects are supposed to be in free space. This is because metals are usually orders of magnitude more conductive than common background media. In environmental or archaeological applications, on the other hand, conductivity contrasts are lower, and therefore the background must be considered together with the targets. This is also a complicated task, mainly because magnetic dipole sources are quite localized and generate 3D fields, and also because in many cases a great number of data has to be modelled. For these reasons, even today, the usual approach to quantitatively interpret EMI data is to apply 1D inversion methods (e.g. Huang and Won 2000, Farquharson *et al* 2003). The use of these methods brings more information than the mere observation of data and gives very good results when the soil structure can be regarded as being approximately 1D. Also, 2D and 3D forward and inversion methods have been developed to reconstruct the conductivity profiles from EMI data, in the absence of highly conductive targets (e.g. Newman and Alumbaugh 1997, Pérez-Flores *et al* 2001, Haber *et al* 2004, Sasaki and Meju 2006, Pellerin and Wannamaker 2005, Martinelli *et al* 2006), but they are usually applied to scales larger than the one required for near-surface studies. In these studies, large areas usually have to be mapped with high lateral and vertical resolution. These conditions imply such a number of data that makes the application of 3D or even 2D inversions too time consuming. Hence, 1D methods are used instead because as they are extremely fast, they allow for evaluating the data in reasonable times.

In this work, we present the results of a study performed to analyse how the instrument orientation affects the ability of the EMI method to detect localized 2D structures, buried at shallow depths, and the possibility of adequately characterizing these targets through 1D inversions. First, we performed a survey at a test site that contains two known structures of this kind, buried in nearly perpendicular directions. We carried out prospection lines approximately parallel to the strike direction of each structure. In each case, we employed, aside from the most common configuration, which corresponds to horizontal coils with the instrument axis parallel to the acquisition lines, several other configurations with horizontal and vertical coils, and with the instrument axis parallel and perpendicular to the lines. We also performed a geoelectric line over one of the buried structures using the dipole–dipole electrode configuration. The features of the anomalies observed in the graphs of the EMI data strongly depended on the configurations. Considering this, we performed numerical simulations using the 2D forward modelling method presented by Martinelli *et al* (2006), in order to explain the main characteristics of these anomalies. Next, we applied to the data the fast lateral filtering technique used in Martinelli and Osella (2010), to reduce the short-scale spurious fluctuations, which are common in EMI data and improve the visualization of the anomalies associated with the targets. Then, we applied to these filtered data the 1D inversion method developed by Farquharson *et al* (2003) and evaluated which configurations provided better estimations of the characteristics of the targets. Finally, we inverted the geoelectric data acquired above one of the targets, using the 2D method by Loke and Barker (1996), compared the obtained subsoil image with the EMI results, and analysed why each method detects this target differently. The conclusions of this analysis were complemented by numerical simulations performed using the same 2D geoelectric inversion code.

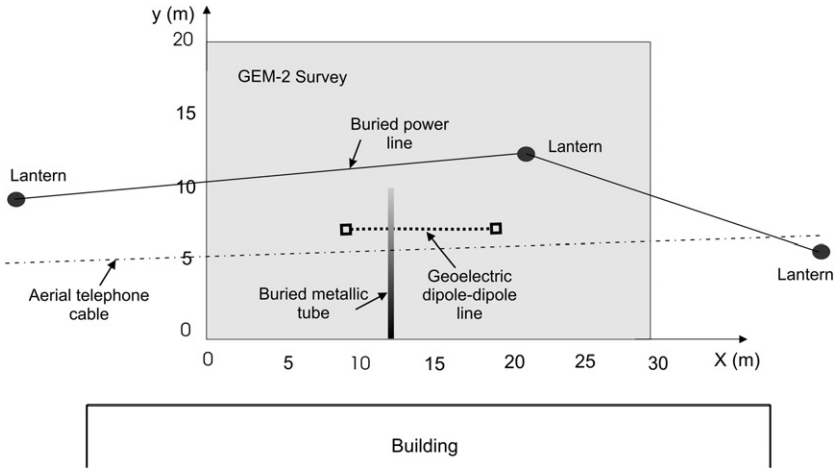

Figure 1. Schematic plan-view of the survey area.

2. Site description and data acquisition

For the EMI survey, we used a GEM-2 equipment (Won *et al* 1996) manufactured by Geophex. These systems are basically composed of two coplanar small coils, a transmitter (Tx) and a receiver (Rx), which are separated by 1.66 m and are moved along acquisition lines at an approximately constant height. Usually, the coils are horizontal and the instrument axis is parallel to the lines. The secondary magnetic field at the receiver is separated into in-phase (IP) and quadrature (Q) components, which are expressed in parts per million (ppm) against the primary field at the receiver. From these components, the apparent conductivity (σ), or its inverse the apparent resistivity ($\rho = 1/\sigma$), and the phase of the secondary field (ϕ) can be calculated as described in the work by Huang and Won (2000). These instruments permit acquiring great numbers of data relatively fast. In their normal, continuous acquisition mode, they typically perform ten measurements per metre. Thus, a dense covering of the surveyed areas can be obtained, which is ideal for near-surface studies. Operation frequencies range from 330 to 47 970 Hz. A maximum of fifteen simultaneous frequencies can be used, but usually no more than six are recommended to ensure good signal-to-noise ratio.

Figure 1 shows a scheme of the studied site, which is in a fill zone close to a riverbank. This site contains two known, localized 2D structures: a metallic tube of diameter 25 cm with a thin insulating coating, ending approximately at $y = 9$ m, and a plastic tube of diameter 5 cm containing electric cables. Both objects are buried approximately 0.8–1.2 m deep. The soil is flat and is covered with slight grass. The first few metres correspond to the filling material, mainly silty loam with some content of river gravel. We prospected a 30 m × 20 m area, acquiring data along parallel lines spaced 1 m, in two perpendicular directions coincident with those of the x- and y-axes, respectively. These acquisition directions correspond to limit cases in which the lines are almost parallel or perpendicular to the targets. It is important to note that the responses corresponding to intermediate directions probably fall in between the ones obtained for these limit cases. In total,

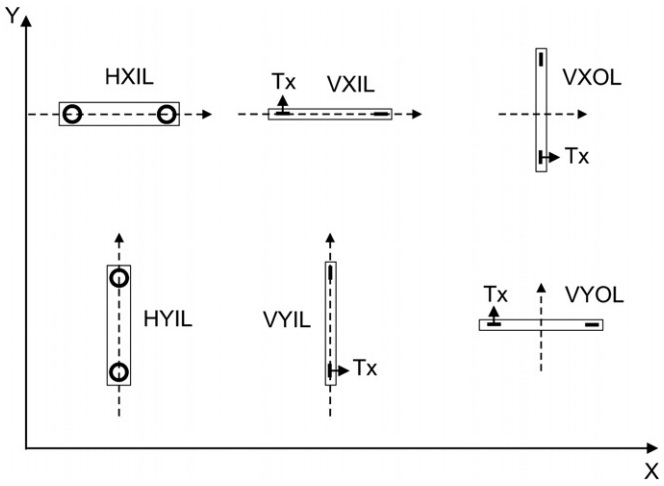

Figure 2. The different configurations used for the GEM-2 survey. The dashed lines indicate the acquisition directions and the small arrows represent the dipole moment of the transmitter, Tx.

we employed six different measurement configurations, which are shown in figure 2. The first character in the configuration names indicates the coil orientation (horizontal, H, or vertical, V), the second the survey line direction (X or Y, for lines parallel to the x- and y-axes, respectively) and the last two the direction of the instrument axis, which can be parallel (in-line, IL) or perpendicular (off-line, OL) to the lines. Considering the involved depths, we employed the frequencies 47 025, 30 375, 20 175, 13 575, 8775 and 5825 Hz.

The geoelectrical profile was performed with a Saris 500 equipment (Scintrex), using the dipole–dipole electrode configuration with aperture $a = 0.5$ m and maximum value of $n = 7$.

3. Analysis of the graphs of the EMI data

As usual, we first performed 2D plan-views of the IP, Q, ρ and ϕ values recorded at each frequency, for each configuration. Figures 3–8 show, as examples, the graphs of ρ obtained

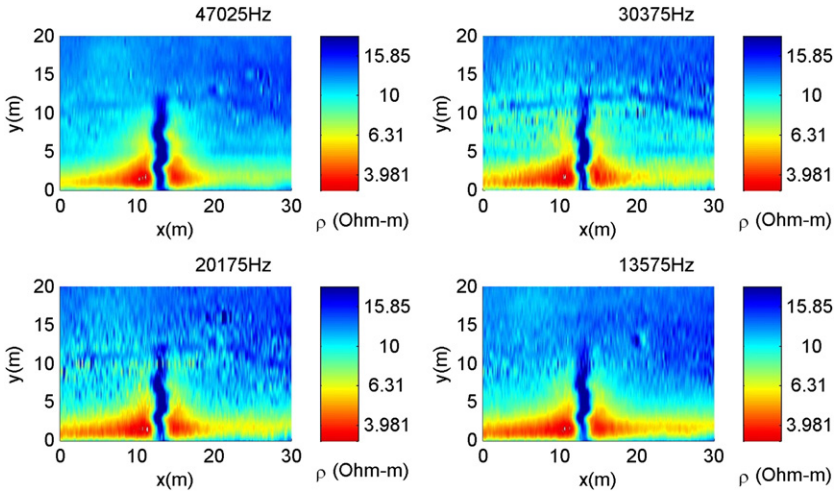

Figure 3. Plan-views of apparent resistivity corresponding to the configuration HXIL, at four representative frequencies.

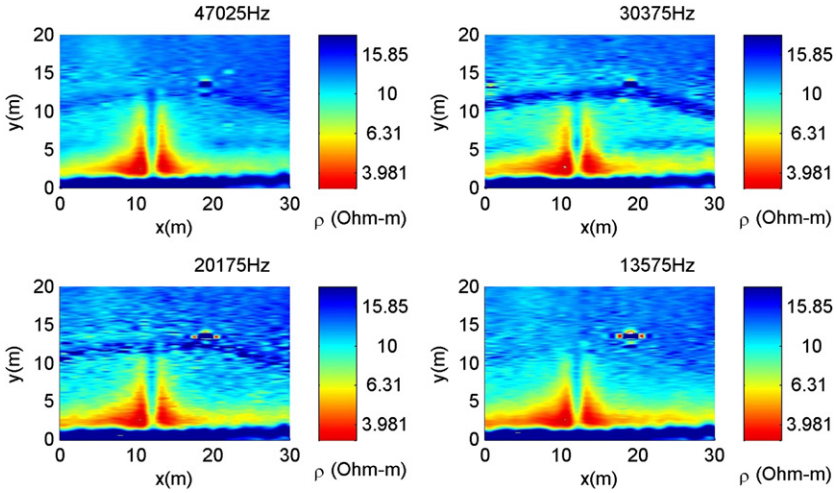

Figure 4. The same as in figure 3, for the configuration HYIL.

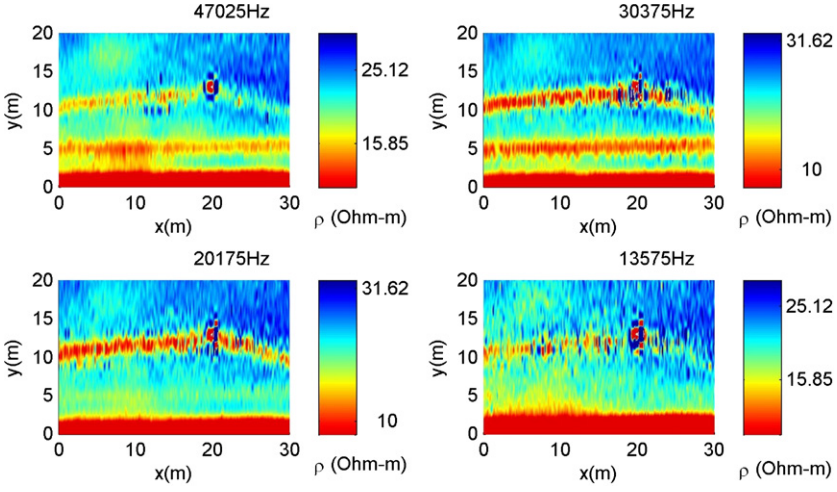

Figure 5. The same as in figure 3, for the configuration VXIL.

for the different configurations, at the first four frequencies, which are representative of the type of anomalies observed at the site. Several interesting conclusions can be drawn from the observation of these graphs. The most important is that the features of the anomalies strongly depend on the instrument orientation. The responses of configurations

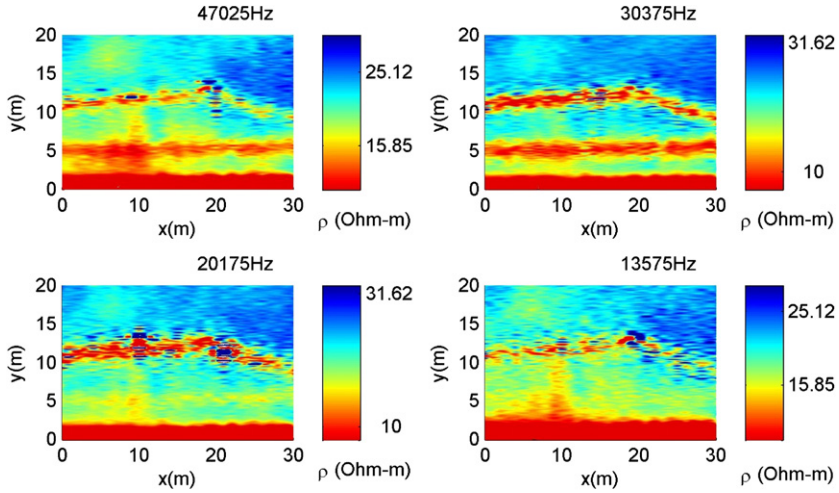

Figure 6. The same as in figure 3, for the configuration VYOL.

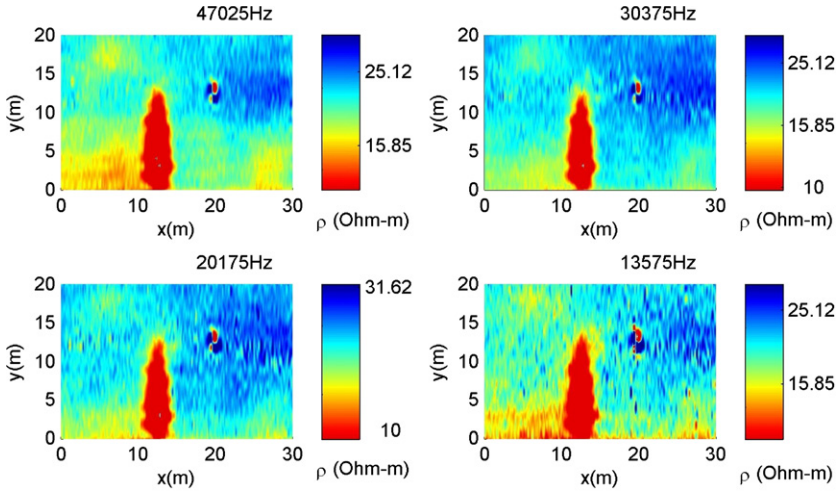

Figure 7. The same as in figure 3, for the configuration VXOL.

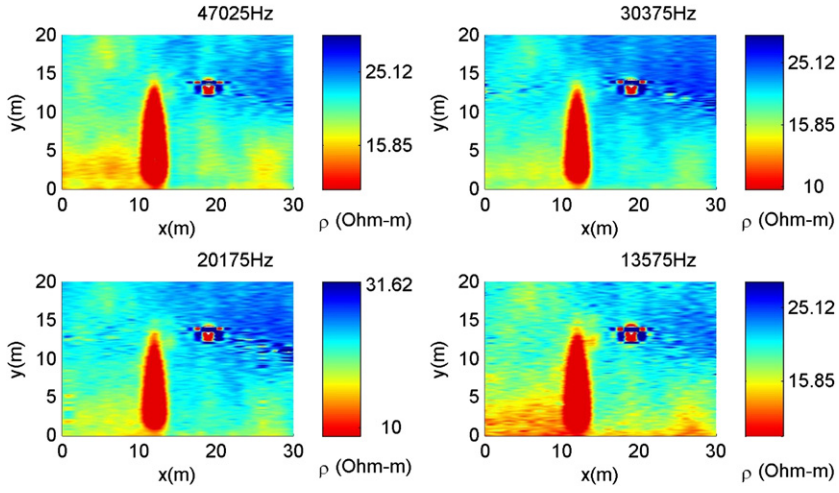

Figure 8. The same as in figure 3, for the configuration VYIL.

with the same instrument orientation but different acquisition directions, such as VXIL and VYOL (figures 5 and 6) or VXOL and VYIL (figures 5 and 6), only present minor differences, which basically correspond to short-scale variations along the measurement direction. As shown later, they can be greatly reduced by applying lateral filtering techniques like the ones

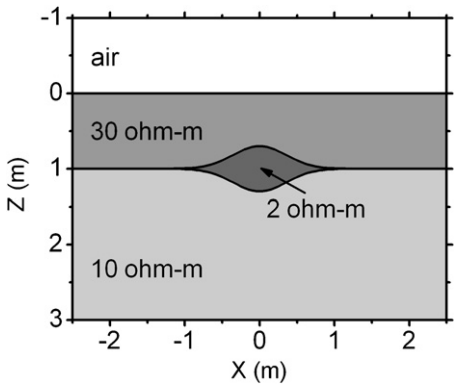

Figure 9. Schematic model of a localized, 2D conductive body.

proposed in Martinelli and Duplaá (2008) and Martinelli and Osella (2010).

The nearby building generates noticeable distortions in the responses of the configurations HXIL, HYIL, VXIL and VYOL, at all the frequencies, up to about $y = 3$–4 m. The characteristics of these distortions are similar to the ones encountered by Martinelli and Osella (2010) in a survey performed at a chemical plant. The greatest effects are observed close to $y = 0$ m, when both the coils and the instrument axis are either perpendicular (configuration HYIL) or parallel (configurations VXIL and VYOL) to the building wall. The apparent conductivity markedly decreases in the first case and increases in the second. Besides, another increase of σ is observed at the two higher frequencies for the configurations VXIL and VYOL, when the x–z plane containing the coils passes through the position of the aerial telephone cord (approximately $y = 5$ m).

As seen from figures 5–8, the vertical configurations generate very different responses depending on the instrument orientation. In the configurations VXIL and VYOL, the plane of the coils is almost parallel to the electric cable; these configurations clearly detect this structure and practically do not detect the metallic pipe. Likewise, the configurations VXOL and VYIL, in which the coil plane is parallel to the metallic pipe, detect the pipe but not the electrical cable. In each case, an increase of σ is observed as the coil plane passes through the corresponding target. In contrast, for both horizontal configurations, σ has a minimum over the centre of the targets. The minimum associated with the electrical wire is more pronounced in the configuration HYIL than in HXIL, whilst the one produced by the pipe is stronger in the configuration HXIL. In addition, there are positive anomalies of σ on both sides of the pipe.

The studied targets are highly conductive metallic objects, protected with resistive insulating coatings. These structures are usually detected as conductive by the EMI method, since the time-varying external magnetic field can induce secondary currents in their metallic interior despite the insulation. Besides, as conductive objects are generally associated with positive anomalies of the apparent conductivity, we did not expect to encounter negative anomalies for any configuration. Considering this, we performed a numerical simulation study to investigate if the features of the anomalies could be explained as 2D effects due to the quite localized characteristic of the targets. We calculated the responses of several conductive bodies of about the same size as the targets, buried at similar depths, using the 2D forward modelling method developed by Martinelli *et al* (2006). Next, we discuss in particular the results obtained for the case of the metallic tube, since this target was the one that produced greater anomalies. Figure 9 shows a schematic model, containing a 2D conductive object about 50 cm wide, buried 1 m deep, and figure 10 shows the Q component obtained for this model at one representative frequency, at which the behaviour is similar to that of σ. The conductivity contrasts and boundary slopes in this model were selected low enough so as to ensure good convergence during the numerical calculations while maintaining the most relevant features of the responses.

As seen by comparing figure 10 with figures 3–8, the main characteristics of the synthetic response obtained for each configuration are in good agreement with the behaviour observed in the corresponding data. In particular, the anomaly

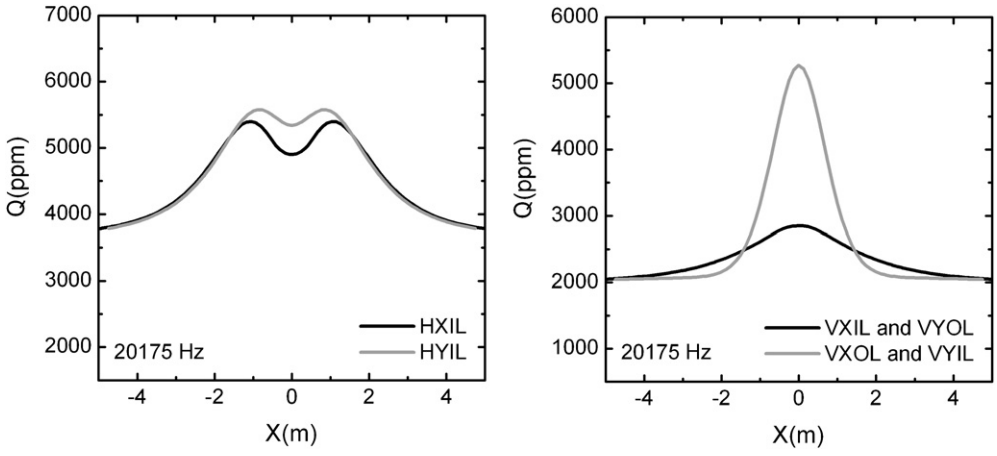

Figure 10. Quadrature component calculated for the model shown in figure 9 using the 2D forward modelling code developed by Martinelli *et al* (2006).

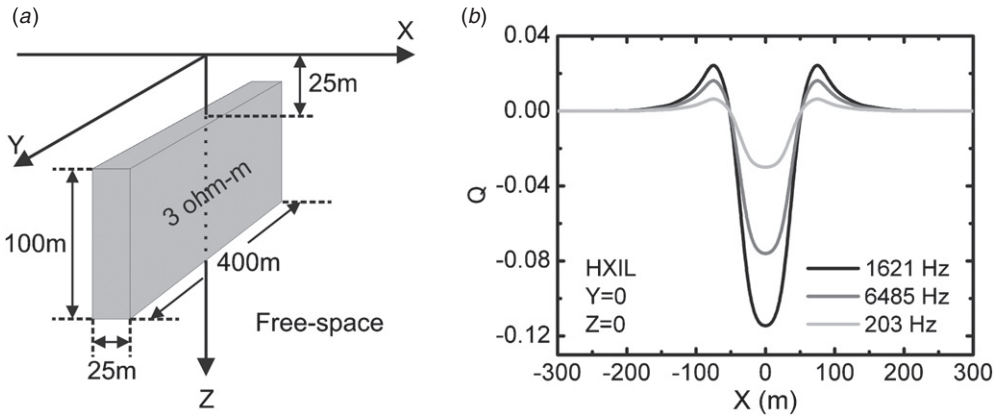

Figure 11. (*a*) A conductive 3D object located in free space. (*b*) Quadrature response of this model along the *x*-axis, for the HXIL configuration. These figures respectively reproduce figures 50(*a*) and 51(*b*) in Frischknecht *et al* (1991).

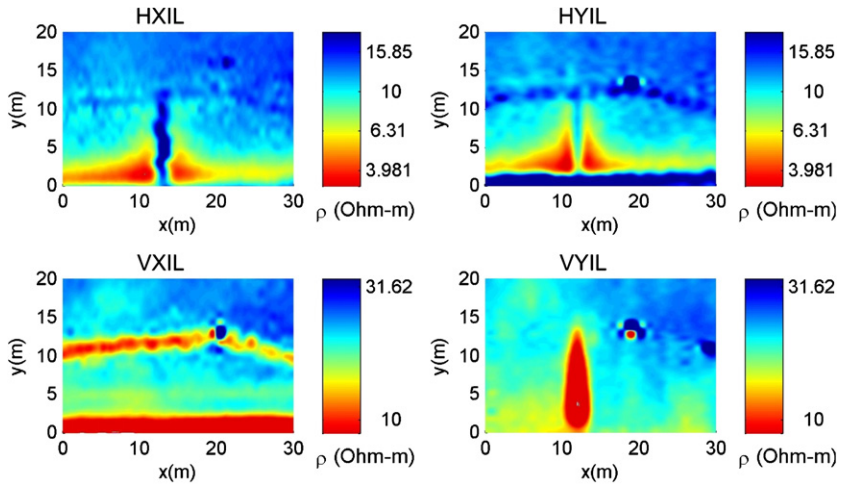

Figure 12. Apparent resistivities obtained at the frequency 20 175 Hz, after applying the spatial filter proposed in Martinelli and Osella (2010), five times, with $\alpha = 2$ and $N = 5$.

of Q obtained for the configurations VXOL and VYIL is positive and much greater than the one obtained for VXIL and VYOL. Besides, for both horizontal configurations, Q also reaches a local minimum over the centre of the conductive body and the minimum corresponding to the HXIL configuration is more pronounced than the one obtained for HYIL. By the last, maxima of Q are observed towards the sides of the body. The main difference with the data is that the Q components of the configurations HXIL and HYIL always remain greater than the reference value corresponding to the host medium, but this is probably related to the fact that the conductivity assigned to the body in the schematic model is quite a bit lower than the actual conductivity of the targets. Then, the results of the 2D modelling seem to indicate that the attributes of the anomalies generated by the pipe are mainly determined by the localized and conductive character of this 2D target and not by the existence of the insulating coating. For completeness, it is important to mention that the inclusion of a resistive medium inside the conductive body in the schematic model does not significantly modify the results.

Frischknecht *et al* (1991) calculated the synthetic responses of many conductive 2D and 3D objects in highly resistive hosts, for different measurement configurations. The results corresponding to several of those models are also consistent with the general behaviour observed in our data. In particular, in figure 11, we reproduce one of those models, together with its Q response for a line corresponding to the HXIL configuration, which crosses just over its centre. Most interesting is that, in this case, the negative absolute minima of Q are effectively obtained over the body.

4. Lateral filtering of the EMI data

The data exhibited detectable amounts of short-scale, spurious lateral variations along the acquisition directions. These variations are common in EMI data acquired with portable instruments carried by an operator, like the GEM-2 equipment used in this case. Aside from EM noise, they are mostly associated with unwanted movements of the instrument during the measurement process and changes in the walking speed of the operator. In previous works, we proposed 2D (Martinelli and Osella 2010) and 3D (Martinelli and Duplaá 2008) fast lateral filters that allow for reducing these variations and improve the visualization of the anomalies produced by the

targets. In this case, we applied to IP, Q, $\log(\rho)$ and ϕ, the filter detailed in Martinelli and Osella (2010), five times, with $\alpha = 2$ and $N = 5$. As an example, in figure 12, we show the results obtained for ρ, at the frequency 20 175 Hz, for the four IL configurations.

5. 1D inversion of the EMI data

We inverted the original and the filtered IP and Q components corresponding to the IL configurations using the 1D inversion code EM1DFM proposed by Farquharson *et al* (2003). For all the configurations, the inversion of the filtered Q component provided the best results.

For the forward modelling, the EM1DFM method uses the matrix propagation approach. During the inversion, at each sounding point, it minimizes a combination of the misfit and the roughness of the 1D model, β being the trade-off parameter that controls the balance between these two quantities. Then, by stitching together these 1D models, pseudo 2D or 3D electrical images of the subsoil can be obtained. These models are smooth in the vertical direction but usually contain sharp lateral variations. Some of these variations denote real changes in the subsoil, but others denote artefacts associated, on one hand, with the short-scale variations of the data previously described and, on the other hand, with variations in the misfits attained in the 1D inversions. We could reduce the lateral changes attributable to misfit variations by using, amongst the different inversion procedures provided by the inversion code, the one that considers a constant, user-supplied value of the trade-off parameter β. A value of $\beta = 500$ provided a good compromise between vertical and lateral variations allowed in the models. In addition, the inversion of the filtered data generated models with fewer lateral variations than the ones obtained from the original data. This is consistent with the results of previous works (Martinelli and Duplaá 2008, Martinelli and Osella 2010). In particular, the best models were obtained from the filtered Q component. The initial models were uniform half-spaces of conductivity 0.002 Siemen m^{-1}, and default values of the parameters α_s^σ, α_z^σ and τ, equal to 0.01, 1 and 0.01, respectively, were selected. The practical depths of investigation were about 5–6 m and were calculated by varying the conductivity of the initial models and then comparing the obtained results.

Figures 13–16 show cuts at different depths of the pseudo 3D electrical images obtained from the 1D inversions of the filtered Q components corresponding to the IL configurations. The models obtained from horizontal coil configurations do not provide an adequate description of the localized targets. The model corresponding to HXIL identifies the metallic pipe as a resistive anomaly, beginning almost at $z = 0$, and barely detects the electrical wire. The model corresponding to HYIL exhibits two conductive anomalies towards the sides of the pipe, again, detectable almost from the earth surface. The electrical cable is detected as a moderate conductive anomaly for $z < 0.7$–0.8 m and as a resistive anomaly for $z < 0.9$–1 m.

The models obtained for the vertical coil configurations give better results. The electrical cable is mainly detected by the configuration VXIL and the pipe by VYIL. In each case, a conductive anomaly is observed. As shown in figure 15, the depth to the top of the electrical cable is rather well determined, about 0.8–0.9 m. Nevertheless, the bottom

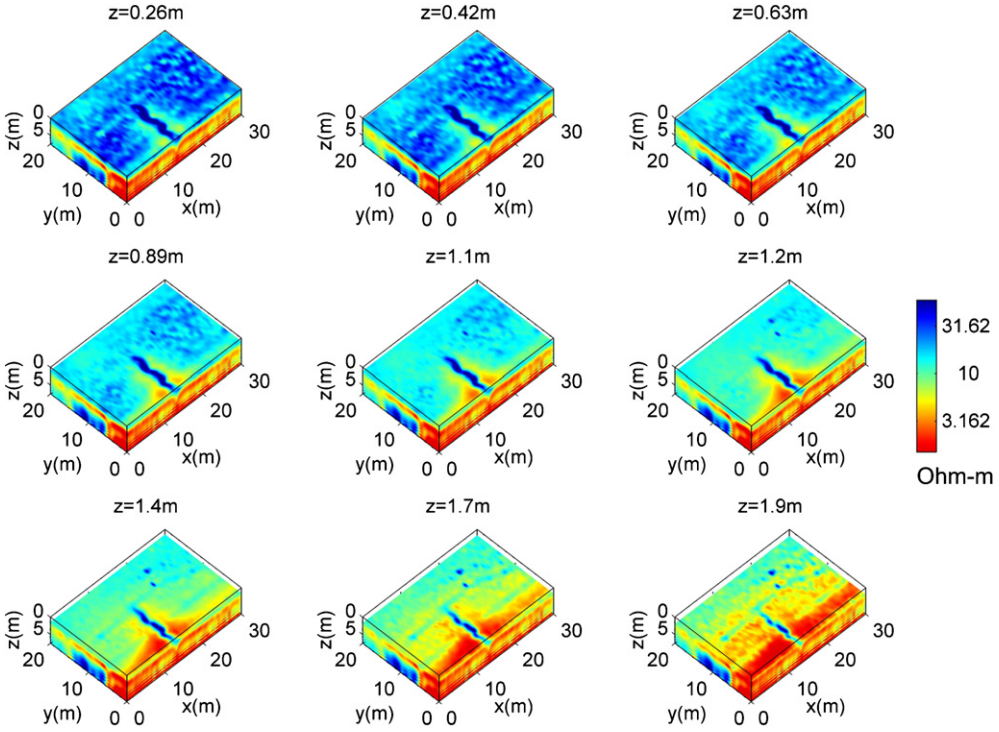

Figure 13. Electrical image obtained from the 1D inversion of the filtered Q component corresponding to the HXIL configuration, performed using the method EM1DFM by Farquharson *et al* (2003).

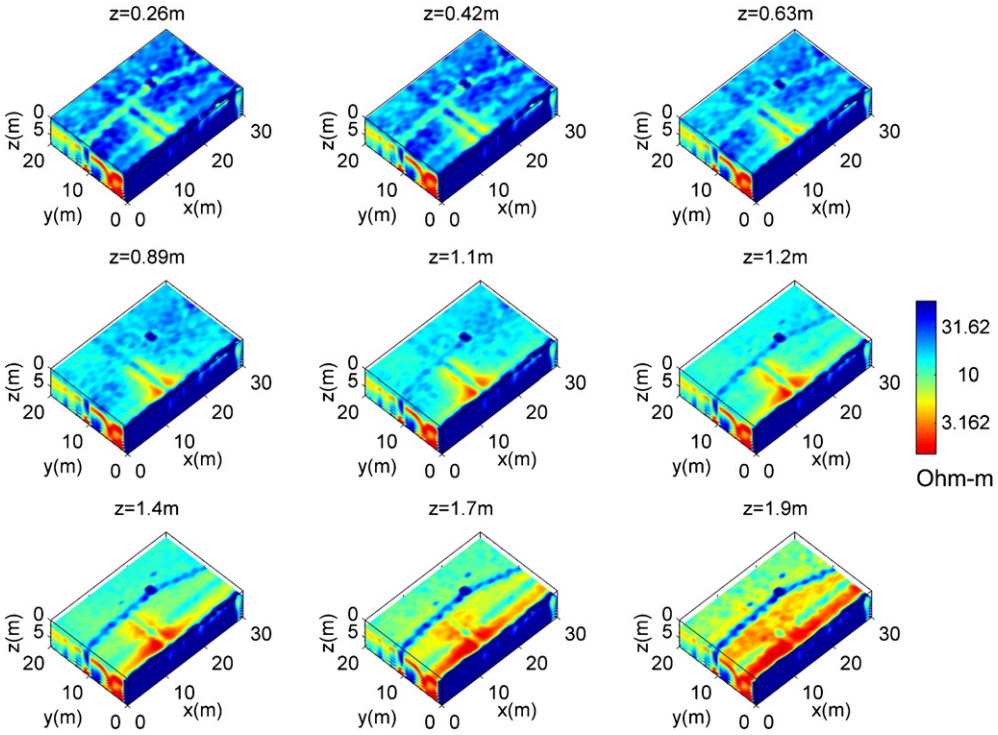

Figure 14. The same as in figure 13, for the configuration HYIL.

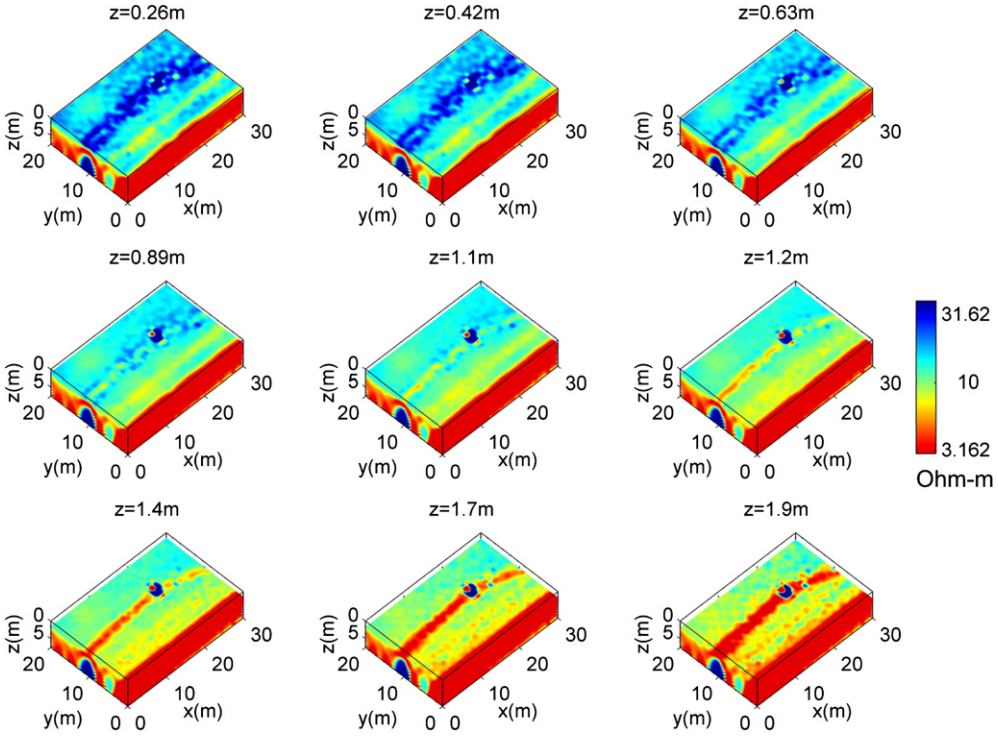

Figure 15. The same as in figure 13, for the configuration VXIL.

of this 2D structure cannot be defined through 1D inversions, since a spurious conductive anomaly appears below the cable that remains for several metres. The anomaly associated with the pipe (figure 16) is perceptible almost from $z = 0$, but the interesting fact is that its conductivity peaks at $z = 0.9$ m, which is close to the actual depth of this target. Once more, the bottom of the pipe is not detected, although the features of the spurious anomaly occurring in this case are somewhat different.

Figure 17 displays the root-mean-squared relative errors corresponding to the inversions shown in figures 13–16. The fittings are in general good, except at the position of

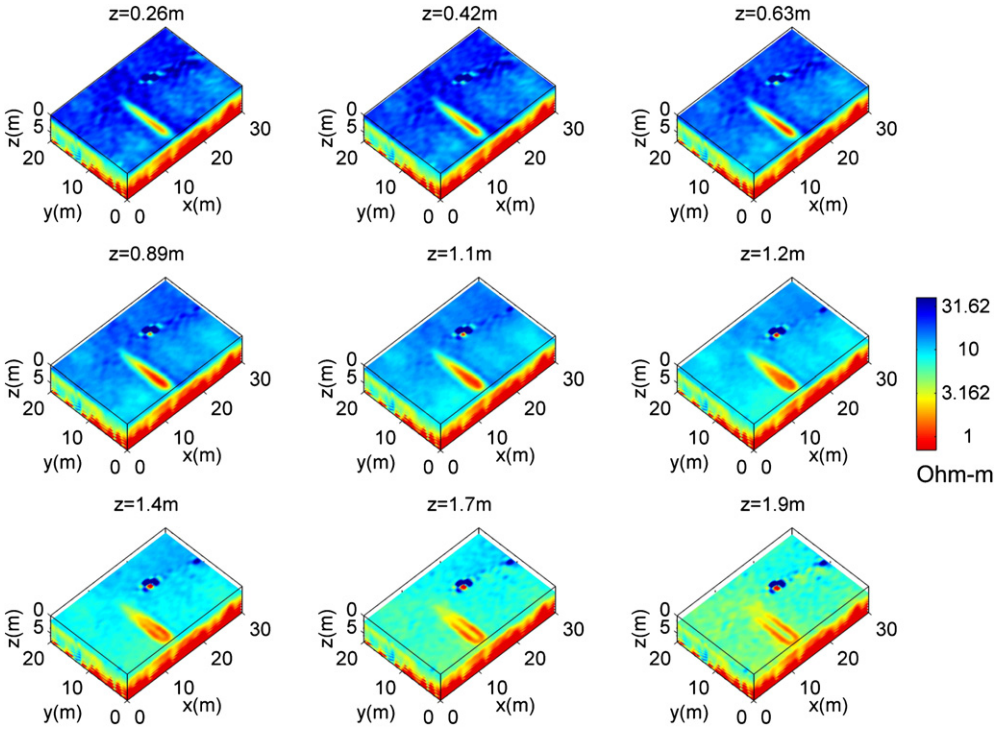

Figure 16. The same as in figure 13, for the configuration VYIL.

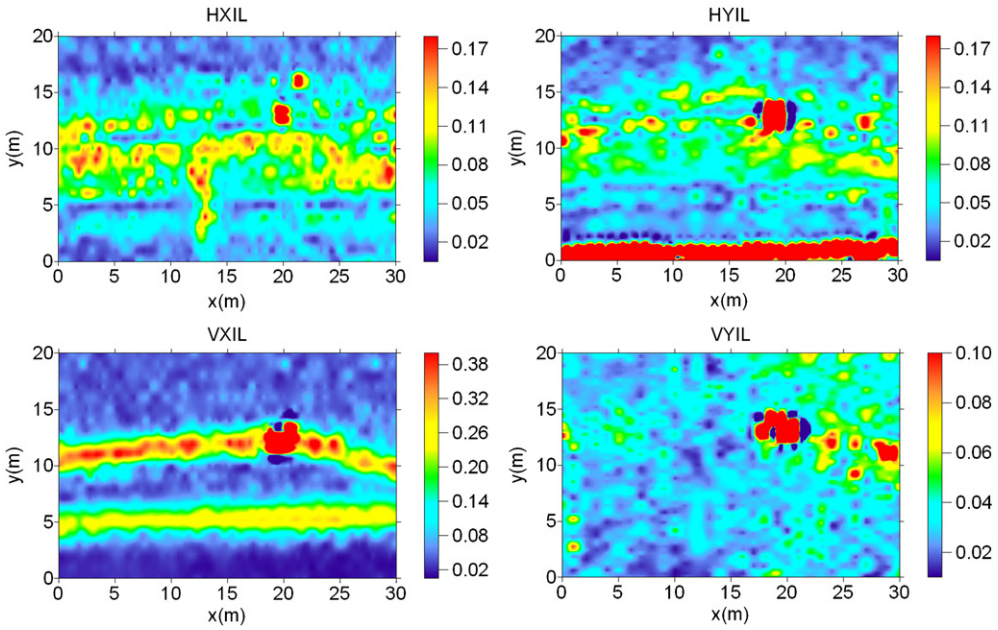

Figure 17. Misfits for the inversions shown in figures 13–16.

the lantern and along the electrical cable for the configuration VXIL.

6. Geoelectrical results

Figure 18 shows the electrical image obtained from the 2D inversion of the dipole–dipole data acquired along the geoelectrical line shown in figure 1. The inversion was performed using the software RES2DINV, based on the work by Loke and Barker (1996). The root-mean-squared relative error, achieved after seven iterations, is 1.02%. This model gives quite a good characterization of the pipe, which crosses this profile near $x = 3.6$ m and is approximately 0.8–0.9 m deep. As discussed before, the EMI method detects the pipe as a conductive object because inductive currents can be generated in the metal in spite of the insulation. In contrast,

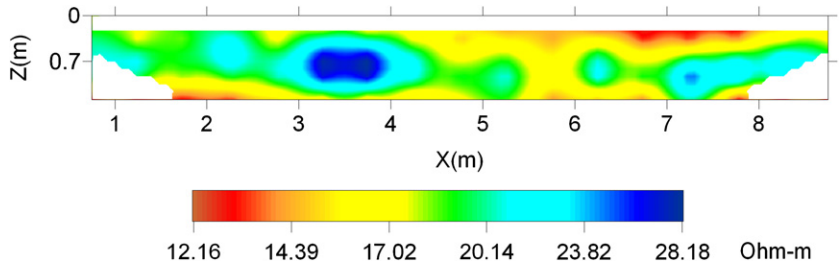

Figure 18. Electrical image obtained from the 2D inversion of the dipole–dipole geoelectrical data, performed using the code RES2DINV (Loke and Barker 1996). The RMS error is 1.02%.

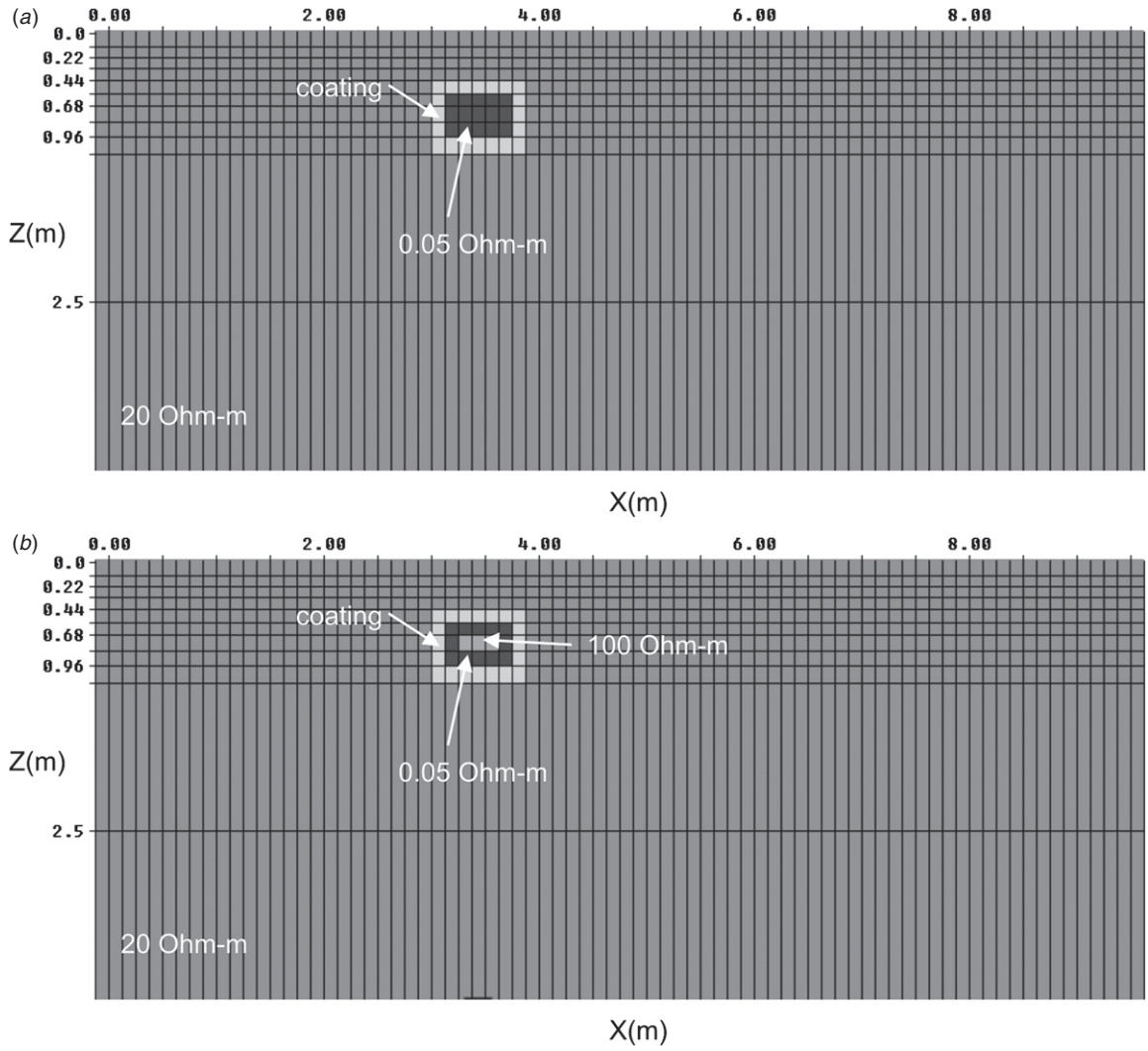

Figure 19. Schematic 2D models representing conductive objects with resistive insulating coatings: (*a*) solid conductor, (*b*) hollow conductor with a resistive medium inside.

this method perceives the pipe as resistive because, due to the insulation, the galvanic currents injected into the soil barely reach the metal.

In general, the resistivity of the anomaly produced by a metallic body with a resistive coating, in the geoelectrical images, increases as the resistivity of the coating increases, and accordingly, the protection of the metallic object against galvanic currents improves. We performed several numerical simulations to investigate the dependence of the anomalies on the coating resistivity, in the particular case of structures similar to the studied pipe. The two selected schematic models are shown in figure 19. First, we calculated the synthetic dipole–dipole responses of these models for different resistivities of the coating, and the same values of a and n maximum as in the data; then, we performed 2D inversions of these responses. Like before, the calculations were performed with the program RES2DINV. The images corresponding to both models were nearly coincident. In figure 20, we show some of the results obtained for the upper model (figure 19(*a*)). In general, the structures are detected as

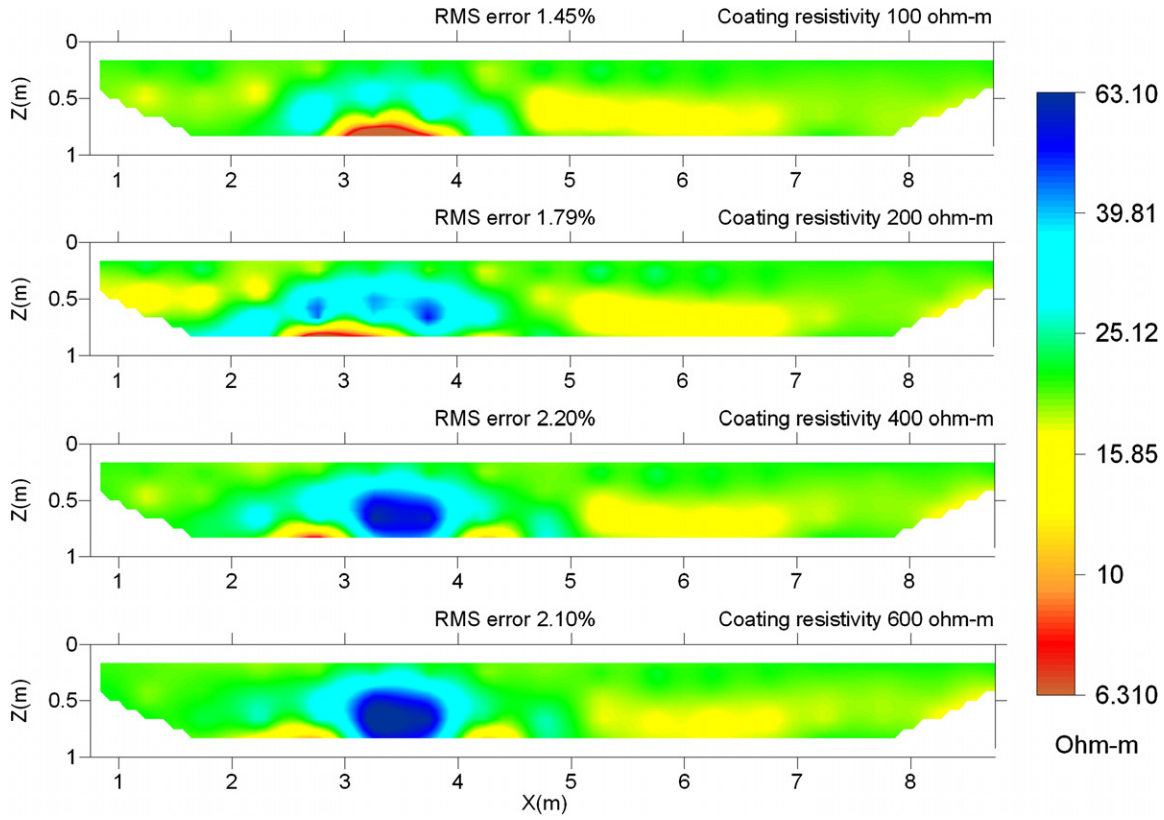

Figure 20. Electrical images obtained from the inversion of the synthetic dipole–dipole geoelectrical responses of the model shown in figure 19(*a*), for different resistivities of the coating. Again, the forward and inverse modellings were performed with the code RES2DINV (Loke and Barker 1996).

well-defined, localized, resistive anomalies for coating resistivities greater than, approximately, 300 Ω m.

7. Conclusions

In this work, we analyse how the system orientation used in EMI surveys affects the capacity to detect near-surface, localized 2D structures, and the ability of obtaining reliable information about this kind of target through 1D inversions. The structures at the studied site are a metallic pipe with a thin insulating coating and a plastic tube containing electric cables; they are buried in two almost perpendicular directions. As explained, we performed parallel prospection lines, approximately in the direction of each structure, with horizontal and vertical coil orientations and the instrument axis parallel and perpendicular to the lines. This allowed us to determine that the characteristics of the anomalies in the apparent conductivity data generated by the targets strongly depend on the instrument orientation. The vertical coil configurations generate completely different responses for the two different orientations of the instrument axis. In each case, basically only the target aligned with the instrument axis is detected, as an important positive anomaly. The differences between the responses obtained with the horizontal coil configurations are quite a bit lower. In both configurations, a decrease of the apparent conductivity is observed just over the targets. The results of numerical simulations performed for the case of the metallic pipe, using a 2D forward modelling method, suggest that the particularities of the anomalies generated by this structure mainly constitute 2D effects associated with its localized character, and also that the presence of the resistive coating does not exert significant effects on the responses.

Then, we performed 1D inversions of the data corresponding to each configuration and drawing together the results generated pseudo 3D models of the subsoil. The images obtained for horizontal coils provide misleading descriptions of the subsoil structure, while the models obtained for vertical coils are quite a bit better, especially up to the depths of the targets. These adequately detect the targets as conductive structures and provide a rather good estimation of their depths.

Finally, the image obtained from the 2D inversion of geoelectrical data acquired along a line crossing the pipe indicates that this method identifies this structure as a resistive object. This does not contradict the EMI results and simply shows that due to the resistive insulating coating, the galvanic currents injected into the ground practically do not reach the metal. In contrast, inductive currents can be generated in the metal in spite of the insulation. We performed some basic numerical simulations to investigate how the anomaly produced by the pipe in the geoelectrical images would change, depending on the coating resistivity. The results obtained for the proposed simplified model seem to indicate that for coating resistivities greater than about 300 Ω m, the pipe would be detected as a well-defined, localized, resistive anomaly.

Acknowledgments

This work was partially supported by CONICET (National Council of Scientific and Technical Research) and ANPCYT (National Agency for Scientific and Technological Promotion). We specially thank Colin G Farquharson, Douglas W Oldenburg and Partha S Routh, for providing us a copy of the code EM1DFM free of charge.

References

Auken E, Pellerin L, Christensen N B and Sørensen K 2006 A survey of current trends in near-surface electrical and electromagnetic methods *Geophysics* **71** G249–60

Bongiovanni M V, Bonomo N, de la Vega M, Martino L and Osella A 2008 Rapid evaluation of multifrequency EMI data to characterize buried structures at a historical Jesuit mission in Argentina *J. Appl. Geophys.* **64** 37–46

Butler D K 2004 Report on a workshop on electromagnetic induction methods for UXO detection and discrimination *Leading Edge* **23** 766–70

Coria D, Bongiovanni V, Bonomo N, de la Vega M and Garea M T 2009 Hydrocarbon contaminated soil: geophysical–chemical methods for designing remediation strategies *Near Surf. Geophys.* **7** 227–36

Farquharson C G, Oldenburg D W and Routh P S 2003 Simultaneous 1D inversion of loop–loop electromagnetic data for magnetic susceptibility and electrical conductivity *Geophysics* **68** 1857–69

Frischknecht F C, Labson V F, Spies B R and Anderson W L 1991 Profiling methods using small sources *Electromagnetic Methods in Applied Geophysics: Applications, Parts A and B* vol 2 ed M N Nabighian (Tulsa, OK: Society of Exploration Geophysicists) Chapter 3 pp 105–270, p 972

Haber E, Ascher U M and Oldenburg D W 2004 Inversion of 3D electromagnetic data in frequency and time domain using an inexact all-at-once approach *Geophysics* **69** 1216–28

Huang H and Won I 2000 Conductivity and susceptibility mapping using broadband electromagnetic sensors *J. Environ. Eng. Geophys.* **5** 31–41

Lascano E, Martinelli P and Osella A 2006 EMI data from an archaeological resistive target revisited *Near Surf. Geophys.* **4** 395–400

Loke M H and Barker R D 1996 Rapid least-squares inversion of apparent resistivity pseudosections by a quasi-Newton method *Geophys. Prospect.* **44** 131–52

Martinelli H P and Osella A M 2010 Small-loop electromagnetic induction for environmental studies at industrial plants *J. Geophys. Eng.* **7** 91–104

Martinelli P and Duplaá M C 2008 Laterally filtered 1D inversions of small-loop, frequency-domain EMI data from a chemical waste site *Geophysics* **73** F143–9

Martinelli P, Osella A and Lascano E 2006 Modeling broadband electromagnetic induction responses of 2-D multilayered structures *IEEE Trans. Geosci. Remote Sens.* **44** 2454–60

McNeill J D 1980 Electromagnetic terrain conductivity measurement at low induction numbers *Geonics Limited, Technical Note* TN-6

McNeill J D and Bosnar M 1999 Application of dipole-dipole electromagnetic systems for geological depth sounding *Geonics Limited, Technical Note* TN-31

Miller J T, Bell T H, Soukup J and Keiswetter D 2001 Simple phenomenological models for wideband frequency-domain electromagnetic induction *IEEE Trans. Geosci. Remote Sens.* **39** 1294–8

Mitsuhata Y, Toshihiro U, Matsuo K, Marui A and Kusunose K 2006 Various-scale electromagnetic investigations of high-salinity zones in a coastal plain *Geophysics* **71** 167–73

Newman G A and Alumbaugh D L 1997 Three-dimensional massively parallel electromagnetic inversion: I. Theory *Geophys. J. Int.* **128** 345–54

Osella A, de la Vega M and Lascano E 2005 3D electrical imaging of an archaeological site using electrical and electromagnetic methods *Geophysics* **70** G101–7

Pellerin L and Wannamaker P 2005 Multi-dimensional electromagnetic modeling and inversion with application to near-surface earth investigations *Comput. Electron. Agric.* **46** 71–102

Pérez-Flores M A, Méndez-Delgado S and Gómez-Treviño E 2001 Imaging low-frequency and dc electromagnetic fields using a simple linear approximation *Geophysics* **66** 1067–81

Sasaki Y and Meju M A 2006 A multidimensional horizontal-loop controlled-source electromagnetic inversion method and its use to characterize heterogeneity in aquiferous fractured crystalline rocks *Geophys. J. Int.* **166** 59–66

Sheard S N, Ritchie T J, Christopherson K and Brand E 2005 Minning, petroleum and engineering industry applications of electromagnetic techniques in geophysics *Surveys Geophys.* **26** 653–69

Sun K, O'Neill K, Shubitidze F, Shamatava I and Paulsen K D 2004 Theoretical analysis and range of validity of TSA formulation for application to UXO discrimination *IEEE Trans. Geosci. Remote Sens.* **42** 1871–81

Witten A J, Calbert G, Witten B and Levy T 2003 Magnetic and electromagnetic induction studies at archaeological sites in southwestern Jordan *J. Environ. Eng. Geophys.* **8** 209–15

Won I J 2003 Small frequency-domain electromagnetic induction sensors *Leading Edge* **22** 320–2

Won I J, Keiswetter D A and Bell T H 2001 Electromagnetic induction spectroscopy for clearing landmines *IEEE Trans. Geosci. Remote Sens.* **39** 703–9

Won I J, Keiswetter D A, Fields G R A and Sutton I C 1996 GEM-2: a new multifrequency electromagnetic sensor *J. Environ. Eng. Geophys.* **1** 129–38